

Object Characterization from Spectral Data Using Nonnegative Factorization and Information Theory

J. Piper* V. Paul Pauca[†] Robert J. Plemmons[‡] Maile Giffin[§]

Abstract

The identification and classification of non-imaging space objects, and ultimately the determination of their shape, function, and status, is an important but difficult problem still to be resolved. While ground-based telescopes with adaptive optics technology have been able to produce high-resolution images for a variety of spaced-based objects, current telescope technology is limited for objects in orbits beyond 1,000 km altitude, such as geosynchronous satellites (approx. 36,000 km orbit). An interesting and promising approach to circumvent this limitation is to collect wavelength-resolved spectral reflectance data, rather than spatially-resolved data, which can then be used to determine information such as material composition of an object. Current work has been focused on the determination of material composition (fractional abundances) from spectral traces when the types or classes of composing materials are known a priori. In this paper, we extend previous work to determine not only fractional abundances, but also the classes of composing materials that make up the object, called endmembers. Endmembers are selected using information-theoretic methods. We employ non-negative matrix factorization algorithms for unmixing of spectral reflectance data to find endmember candidates and regularized inverse problem methods for determining corresponding fractional abundances. Promising numerical results are presented using laboratory and simulated datasets.

1 Introduction

The determination of space objects whose orbits are significantly distant (e.g. geosynchronous satellites) or whose dimensions are small (e.g. nanosatellites) is a challenging problem in astronomical imaging. Because of their distant orbits or small dimensions these objects are difficult to resolved spatially using ground-based telescope technology, hence they are denoted as non-imaging objects (NOI). Recently alternate approaches have been proposed in an attempt to circumvent this problem. Among these, the collection and analysis of wavelength-resolved data is a promising and

*Department of Computer Science, Wake Forest University, Winston-Salem, NC 27109. His research was supported in part by the Air Force Office of Scientific Research under grant F49620-02-1-0107. Email: pipejw02@wfu.edu

[†]Department of Computer Science, Wake Forest University, Winston-Salem, NC 27109. His research was supported in part by the Air Force Office of Scientific Research under grant FA49620-03-1-0215, and by the Army Research Office under grant DAAD19-00-1-0540. Email: paucavp@wfu.edu

[‡]Departments of Computer Science and Mathematics, Wake Forest University, Winston-Salem, NC 27109. His research was supported in part by the Air Force Office of Scientific Research under grant F49620-02-1-0107 and by the Army Research Office under grant DAAD19-00-1-0540. Email: plemmons@wfu.edu

[§]Oceanit Laboratories, 590 Lipoa Parkway Kihei, Maui, HI 96753. Her research was supported in part by the Air Force Office of Scientific Research under grant F49620-02-1-0107. Email: mgiffin@oceanit.com

viable approach currently under investigation. Here an instrument such as the SPICA spectrometer is employed to collect spectral reflectance traces of a space object over a specific period of time.

A fundamental difficulty with this approach is the determination of characteristics of the material that make up an object from its collection of spectral traces. More specifically, it is desired to determine i) the type of constituent material and ii) the proportional amount of these materials that make up the object. The first problem involves the detection of material spectral signatures, or *endmembers* from the spectral data. The second problem involves the computation of corresponding proportional amounts, or *fractional abundances*.

Here, we propose an unsupervised method for detecting endmembers as well as for computing fractional abundances from the spectral reflectance traces of a non-imaging space object. Our methodology extends previous research [3, 10, 12] in at least two ways. It deals with the material spectral unmixing problem numerically by solving an optimization problem with non-negative and smoothness constraints in the data. It then uses the Kullback-Leibler divergence, an information-theoretic measure, to select computed endmembers that best match known materials in the database. Fractional abundances are then computed using the selected endmembers using constrained least squares methods.

Spectral unmixing is a problem that originated within the hyperspectral imaging community and several computational methods to solve it have been proposed over the last few years. A thorough study and comparison of various computational methods for endmember computation, in the related context of hyperspectral unmixing can be found in the work of Plaza *et al.*, [14]. An information-theoretic approach has been provided by Chang [4]. Recently, nonnegative matrix factorization (NMF), proposed by Lee and Seung [9], has been used with relative success in this problem. We extend NMF by considering a class of smoothness constraints on the optimization problem for more accurate endmember computation.

The Kullback-Leibler divergence measure is selected over other methods for matching computed endmembers against material traces stored in a database. It has several advantages over simpler methods, such as the cosine of the angle between material traces. The Kullback-Leibler divergence is an information, or cross-entropy measure that captures the spectral correlation between traces and facilitates more accurate matching and selection of computed endmembers.

This paper is organized as follows. First we introduce the standard [7] linear mixing model for spectral data in Section 2, and relate it to our application. Our novel techniques for endmember extraction, selection, and quantification are described in Section 3. Results from some extensive numerical simulations studies are provided in Section 4. These computations illustrate the effectiveness of our techniques.

2 The Linear Mixing Model

We assume that a spectral trace is a linear combination of a set of endmembers, weighted by corresponding material quantities or fractional abundances. The assumption of a linear process is a powerful and typical choice taken in many hyperspectral imaging applications [7]. Let s_i ($1 \leq i \leq p$) be endmembers corresponding to different material spectral signatures. Each endmember s_i is a vector containing nonnegative spectral measurements along m different spectral bands. Then, an observed spectral trace \mathbf{y} can be expressed as

$$\mathbf{y} = S\mathbf{x} + \mathbf{n}, \tag{1}$$

where $S = [\mathbf{s}_1 \ \dots \ \mathbf{s}_p]$ is an $m \times p$ matrix whose columns are the endmembers, \mathbf{x} is a vector of fractional abundances, and \mathbf{n} is an additive observation noise vector. Moreover, $\mathbf{x} \geq 0$ and $\sum \mathbf{x}_i = 1$.

When a sequence of n time-varying spectral traces $\{y_i\}$ is considered, matrix notation is appropriate to express all traces as

$$Y = SX + N, \quad (2)$$

where

$$Y = [\mathbf{y}_1 \ \dots \ \mathbf{y}_n], \quad X = [\mathbf{x}_1 \ \dots \ \mathbf{x}_n], \quad N = [\mathbf{n}_1 \ \dots \ \mathbf{n}_n]. \quad (3)$$

Previous work by Luu *et al.* [10] has demonstrated the effectiveness of the linear mixing model in non-imaging space object characterization. In this work, a dataset of laboratory-obtained spectral signatures of several classes of materials, such as aluminum, solar cell, mylar and white paint, is employed to form an artificial endmember matrix S and spectral traces are generated from the endmembers and stored as the columns of the matrix Y . A constrained least square method is then used, given Y and S , to compute an approximation to X . Here, we do not assume *a priori* knowledge of S in the computation of fractional abundances. Rather we extend the work of Luu *et al.* by first computing an approximation matrix, which we denote by B , to S using only knowledge of the matrix Y . An inverse problem is then subsequently solved for X , given Y and B . Knowledge of the laboratory-obtained spectra is used only in the selection of endmembers to form B .

3 Endmember Extraction, Selection, and Quantification

In this section, we introduce a novel approach for both extracting endmembers and computing fractional abundances from spectral data. This approach consists of three key sequential steps which can be summarized as *extract*, *select*, and *quantify*. That is, first extract possible endmembers in a matrix W from the observed data matrix Y . Second, select columns of W using information-theoretic metrics and the dataset of laboratory-obtained spectral traces to form a matrix $B \approx S$. Third, use B and Y to quantify the matrix X in terms of material fractional abundances. Next, we describe in detail our proposed approach.

Proposed Methodology

1. **Extract W from Y .** We solve a constrained optimization problem,

$$\min_{W, H} \{ \|Y - WH\|_F^2 + \alpha J_1(W) + \beta J_2(H) \}, \quad (4)$$

for $W \geq 0$ and $H \geq 0$, where $\|\cdot\|_F$ is the Frobenius norm, the columns of $W = [\mathbf{w}_1 \ \dots \ \mathbf{w}_k]$, for some specified value of k , are the possible endmembers, and H is a by-product matrix of mixing coefficients. The functions $J_1(W)$ and $J_2(H)$ are penalty terms used to enforce certain constraints on the solution of Equation (4), and α and β are their corresponding Lagrangian multipliers, or regularization parameters. Different penalty terms may be used depending upon the desired effects on the computed solution. For the current application, we set

$$J_1(W) = \|W\|_F^2, \quad (5)$$

in order to enforce smoothness in W . A similar constraint may be placed on H via $J_2(H)$ to enforce, for example, statistical sparseness [6], which is useful in certain text clustering applications [13].

2. **Select $B \approx S$.** The Kullback-Leibler divergence is an information-theoretic quantity that measures the difference between two probability distributions. We use the Kullback-Leibler divergence pseudo-metric to compute proximity of the columns of W to the material spectral signatures in our laboratory-obtained dataset.
3. **Quantify the fractional abundances.** We solve equation (2) for X using the approximation B in place of S . Methods typically employed for inverse problems are considered, in particular we use a preconditioned version of a modified steepest descent method that enforces nonnegativity on the solution.

3.1 Endmember Extraction Using Nonnegative Matrix Factorizations

Non-negative matrix factorization (NMF) has been shown to be a very useful technique in approximating high dimensional data where the data are comprised of non-negative components. In a seminal paper published in *Nature* [9], Lee and Seung proposed the idea of using NMF techniques to find a set of basis functions to represent image data where the basis functions enable the identification and classification of intrinsic “parts” that make up the object being imaged by multiple observations. Low-rank non-negative matrix factorizations not only enable the user to work with reduced dimensional models, they also often facilitate more efficient statistical classification, clustering and organization of data, and lead to faster searches and queries for patterns or trends, e.g., Pauca, Shahnaz, Berry and Plemmons [13]. Here, we derive a new constrained version of NMF that takes into consideration smoothness constraints.

Let $F(W, H)$ be a scalar-valued function defined by

$$F(W, H) = \frac{1}{2} \|Y - WH\|_F^2 + \frac{\alpha}{2} \|W\|_F^2 + \frac{\beta}{2} \|H\|_F^2. \quad (6)$$

NMF is based on an alternating gradient descent mechanism. That is, for some starting matrices $W^{(0)}$ and $H^{(0)}$, the sequences $\{W^{(t)}\}$ and $\{H^{(t)}\}$, $t = 1, 2, \dots$, are computed by means of the formulas,

$$W_{ij}^{(t)} = W_{ij}^{(t-1)} - \theta_{ij} \frac{\partial F(W, H)}{\partial W_{ij}}, \quad 1 \leq i \leq m, \quad 1 \leq j \leq k \quad (7)$$

$$H_{ij}^{(t)} = H_{ij}^{(t-1)} - \phi_{ij} \frac{\partial F(W, H)}{\partial H_{ij}}, \quad 1 \leq i \leq k, \quad 1 \leq j \leq n. \quad (8)$$

Taking the derivatives of $F(W, H)$ with respect to W_{ij} and H_{ij} and after some algebraic manipulations, the gradients about W_{ij} and H_{ij} can be expressed in matrix-vector form as,

$$\frac{\partial F(W, H)}{\partial W_{ij}} = -YH^T + WHH^T + \alpha W, \quad (9)$$

$$\frac{\partial F(W, H)}{\partial H_{ij}} = -W^T Y + W^T W H + \beta H. \quad (10)$$

The scalar quantities θ_{ij} and ϕ_{ij} determine the lengths of the steps to take along the negative of the gradients about W_{ij} and H_{ij} , respectively, and must be chosen carefully. Hoyer [6] selects

$\theta_{ij} = c_1$ and $\phi_{ij} = c_2$ for some constants c_1 and c_2 . Here we follow Lee and Seung [9] and choose these quantities based on current estimates of W and H ,

$$\theta_{ij} = \frac{W_{ij}^{(t-1)}}{(W^{(t-1)} H H^T)_{ij}}, \quad (11)$$

$$\phi_{ij} = \frac{H_{ij}^{(t-1)}}{(W^T W H^{(t-1)})_{ij}}. \quad (12)$$

Substituting (9), (10), (11), and (12) into (7) and (8), we obtain the following update rules,

$$W_{ij}^{(t)} = W_{ij}^{(t-1)} \cdot \frac{(Y H^T)_{ij} - \alpha W_{ij}^{(t-1)}}{(W^{(t-1)} H H^T)_{ij}} \quad (13)$$

$$H_{ij}^{(t)} = H_{ij}^{(t-1)} \cdot \frac{(W^T Y)_{ij} - \beta H_{ij}^{(t-1)} - \beta H_{ij}^{(t-1)}}{(W^T W H^{(t-1)})_{ij}}. \quad (14)$$

It is not difficult to prove that for our choices of $J_1(W)$ and $J_2(H)$, the function $F(W, H)$ is non-increasing under the updates rules (13) and (14). Next, we summarize our new constrained version of NMF.

Constrained NMF (CNMF)

1. Choose the number of basis vectors k .
2. Initialize $W^{(0)}$ and $H^{(0)}$ with non-negative values.
3. For $t = 1, 2, \dots$, until $F(W^{(t)}, H^{(t)}) \leq \text{tol}$, for a chosen tolerance value $\text{tol} \in \mathbb{R}$, compute

$$(a) \quad H_{cj}^{(t)} \leftarrow H_{cj}^{(t-1)} \frac{\left((W^{(t-1)})^T Y \right)_{cj} - \beta H_{cj}^{(t-1)}}{\left((W^{(t-1)})^T W^{(t-1)} H^{(t-1)} \right)_{cj} + \epsilon}, \quad 1 \leq c \leq k, \quad 1 \leq j \leq n,$$

$$(b) \quad W_{ic}^{(t)} \leftarrow W_{ic}^{(t-1)} \frac{\left(Y (H^{(t)})^T \right)_{ic} - \alpha W_{ic}^{(t-1)}}{\left(W^{(t-1)} H^{(t)} (H^{(t)})^T \right)_{ic} + \epsilon}, \quad 1 \leq i \leq m, \quad 1 \leq c \leq k.$$

where $\epsilon \approx 10^{-9}$ is used to avoid possible division by zero.

The regularization parameters $\alpha \in \mathcal{R}$ and $\beta \in \mathcal{R}$ are used to balance the trade-off between accuracy of the approximation and smoothness of the computed solution and their selection is typically problem dependent. Of course the matrices W and H are generally not unique. Conditions resulting in uniqueness in the special case of equality, $Y = WH$, have been recently studied by Donoho and Stodden [5], using cone theoretic techniques (See also Chapter 1 in Berman and Plemmons [1]). The case where Y is symmetric is studied by Catral, Han, Neumann and Plemmons [2].

3.2 Endmember Selection using Information-Theoretic Techniques

In this section we describe our use of Kullback-Leibler information theoretic measures to select computed endmembers by calculating their proximity to laboratory-obtained spectral signatures of space object material. Related measures have been recently considered in the context of hyperspectral imaging, in particular by Chang [4]. Let a vector $\mathbf{w} \geq 0$ (a column of W) denote a random variable associated with an appropriate probability space. The probability density vector \mathbf{p} associated with \mathbf{w} is given by

$$\mathbf{p} = \frac{1}{\sum w_i} \mathbf{w}. \quad (15)$$

The vector \mathbf{p} can be used to describe the variability of a spectral trace. Moreover, the entropy of each \mathbf{w} can be defined, using base-two logarithms, as

$$h(\mathbf{w}) = - \sum p_i \log p_i, \quad (16)$$

which can then be used to describe the uncertainty [4] in \mathbf{w} . Now, let \mathbf{d} be a laboratory-obtained material spectral signature with probability density vector $\mathbf{q} = (1/\sum d_i)\mathbf{d}$. Then using information theory the relative entropy of \mathbf{d} with respect to \mathbf{w} can be defined by

$$D(\mathbf{w}||\mathbf{d}) = \sum p_i(\log(p_i) - \log(q_i)) = \sum p_i \log\left(\frac{p_i}{q_i}\right), \quad (17)$$

where the quantities $-\log p_i$ and $-\log q_i$ are the self-information measures of \mathbf{w} and \mathbf{d} , respectively, along the i th spectral band. Here, $D(\mathbf{w}||\mathbf{d})$, is known as the Kullback-Leibler divergence (KLD) measure, but it is not symmetric with respect to \mathbf{w} and \mathbf{d} . The following symmetrized version [4] may instead be considered,

$$D_s(\mathbf{w}, \mathbf{d}) = D(\mathbf{w}||\mathbf{d}) + D(\mathbf{d}||\mathbf{w}). \quad (18)$$

In our approach, the *symmetric Kullback-Leibler Divergence* (SKLD) measure (18) is used to compute a confusion matrix $C(W, L)$ between each column \mathbf{w}_i in matrix W and each trace \mathbf{d}_j in a laboratory-obtained dataset L of material spectral signatures. For each \mathbf{d}_j , $\arg \min_{\mathbf{w}_i} C(W, \mathbf{d}_j)$ indicates the endmember candidate in W to which \mathbf{d}_j is closest to in terms of (18). Consequently each material \mathbf{d}_j in L has associated with it some endmember candidate \mathbf{w}_i . A tolerance parameter τ is used to reject endmembers \mathbf{w}_i for which the SKLD is larger than τ . The selected columns of W are then used to form a matrix B . This matrix is subsequently used in the third step of our approach to quantify fractional abundances.

3.3 Quantification of Fractional Abundances

For quantifying fractional abundances, given $B \approx S$, we solve

$$J(X) = \min_X \|Y - BX\|_F^2 \quad (19)$$

subject to nonnegativity constraint $X \geq 0$. A variety of solution techniques can be used. We select PMRNSD, a preconditioned fixed point iteration type approach proposed by Nagy, Palmer, and Perrone [11]. In this approach, the constrained minimization problem is first transformed into an unconstrained problem by parameterizing X as $X = e^Z$.

We consider, without loss of generality, the equivalent case of minimizing (19) one column at the time,

$$J(\mathbf{x}) = \min_{\mathbf{x}} \|\mathbf{y} - B\mathbf{x}\|_2^2, \quad \text{for } \mathbf{x} = e^{\mathbf{z}}. \quad (20)$$

A local non negatively constrained minimizer of (20) can be computed via the fixed point iteration,

$$\mathbf{x}_{k+1} = \mathbf{x}_k + \tau_k \mathbf{v}_k, \quad \mathbf{v}_k = -\text{diag}(\nabla J(\mathbf{x}_k)) \mathbf{x}_k, \quad (21)$$

where $\text{diag}(\nabla J(\mathbf{x}_k))$ is a diagonal matrix whose entries are given by $\nabla J(\mathbf{x}_k) = B^T(\mathbf{y} - B\mathbf{x})$. In the PMRNSD algorithm the parameter τ_k is given by $\tau_k = \min\{\tau_{uc}, \tau_{bd}\}$, where τ_{uc} corresponds to the unconstrained minimizer of J in the direction \mathbf{v}_k and τ_{bd} is the minimum $\tau > 0$ such that $\mathbf{x}_k + \tau \mathbf{v}_k \geq 0$. Circulant type preconditioners are employed to speed up the convergence of the fixed point iteration method [11].

4 Numerical Results

Four satellites were simulated with varying compositions of aluminum, mylar, solar cell, and white paint. The surface of each satellite was composed of 50% of one of the materials and nearly equal amounts of the remaining three materials. These fractional abundances were then allowed to vary sinusoidally with different randomly generated amplitudes, frequencies, and phase shifts, so as to model space object rotation with respect to a fixed detector, such as the SPICA spectrometer. The resulting material fractional abundances and the corresponding laboratory-obtained spectra shown in Figure 1 were used to generate $p = 100$ spectral traces of length $m = 155$ for each satellite using the linear mixing model equation (2), with 1% additive Gaussian noise.

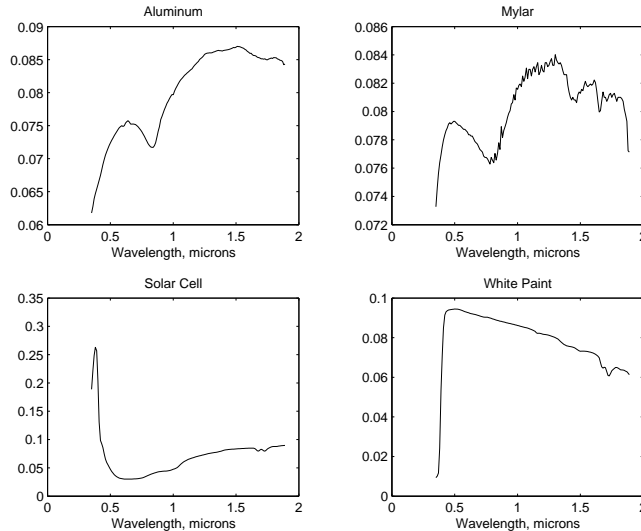


Figure 1: Laboratory spectral traces for the four materials used in data construction: aluminum, mylar, solar cell, and white paint. These spectral traces are in fact averages of several traces of each type of material (see Luu *et al.* [10] for details).

CNMF was then used 20 times to extract $k = 6$ endmembers for a total of 120 endmember candidates for each satellite dataset and for a dataset composed of all four satellites. We set the

regularization parameters $\alpha = 1$ and $\beta = 0$ to enforce smoothness only in W . The SKLD was then computed between each endmember and each material spectrum. For each dataset, the endmember with the smallest SKLD was then selected for each of the four materials. The resulting SKLD scores are shown in Figure 2.

	Aluminum	Mylar	Solar Cell	White Paint
50% Aluminum	0.0233	0.0124	0.4659	0.1321
50% Mylar	0.0165	0.0063	0.4009	0.1203
50% Solar Cell	0.0645	0.0292	0.0302	0.2863
50% White Paint	0.0460	0.0125	0.8560	0.1735
All Four	0.0280	0.0659	0.0130	0.0223

Figure 2: Confusion matrix for best matched CNMF extracted endmember candidates from simulated satellites and laboratory material spectra. Noise was 1% and $\alpha = 1$. Reported is the SKLD. Better matches are closer to 0.

This method could allow one endmember to be the best match for multiple materials, which is reasonable given the difficulty of resolving some materials using CNMF and the SKLD. This can be seen in the similarity of SKLD scores between the laboratory spectra, particularly aluminum and mylar, shown in Figure 3.

	Aluminum	Mylar	Solar Cell	White Paint
Aluminum	0	0.0209	1.2897	0.3317
Mylar	0.0209	0	1.2719	0.2979
Solar Cell	1.2897	1.2719	0	2.5781
White Paint	0.3317	0.2979	2.5781	0

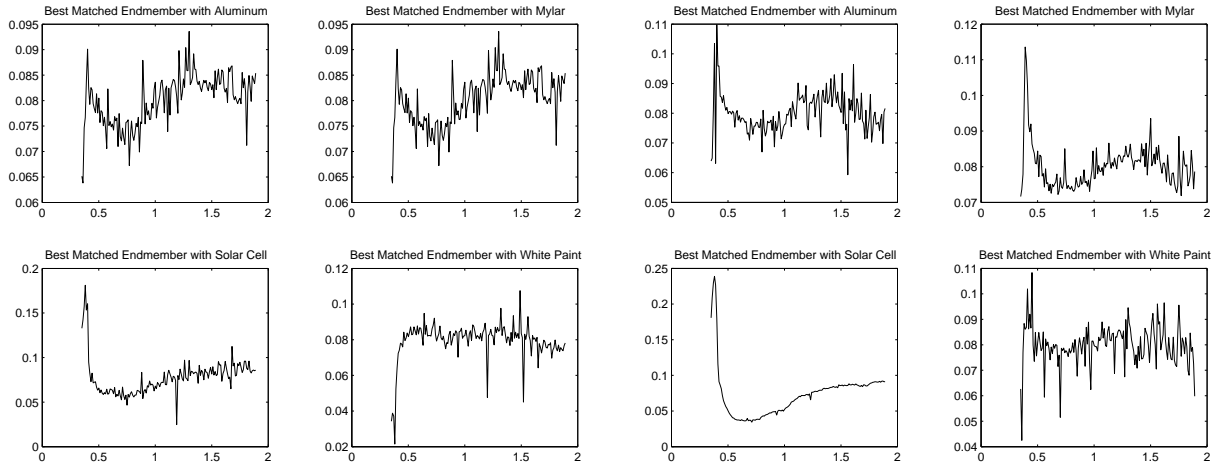
Figure 3: Confusion matrix for laboratory material spectra with each other. Reported is the SKLD.

Using the confusion matrix in Figure 3, reasonable selection thresholds can be defined for each of the four possible materials in the laboratory dataset L . The minimum SKLD from the confusion matrix in Figure 3 was chosen as the threshold, τ . In the case of aluminum and mylar, the SKLD between these two materials was rejected and the minimum of the remaining values was chosen. This decision has the result of including both materials in the matrix B whenever either is present, which could introduce errors when the fractional abundances are subsequently calculated if one were not present. However, choosing $\tau = 0.0209$ would have resulted in aluminum being excluded from B for the satellite dominated by aluminum, and aluminum and mylar being excluded from B for the dataset composed of all four satellites.

Another method for selecting τ is to use simulated satellites which do not have a given material on their surfaces. Calculating the best SKLD for a set of CNMF-obtained endmembers also gives a reasonable τ . The same problem exists in selecting τ for aluminum and mylar as with the previous method. This method for choosing τ results in the same endmember selections for our data as the confusion matrix method. In either case, a suitable endmember is found for each of the four materials in D .

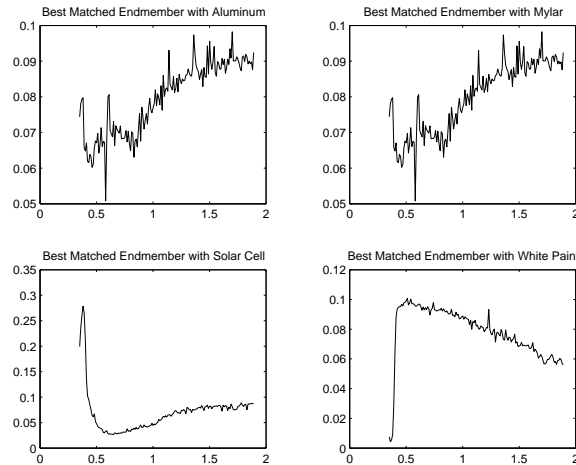
Figure 4 shows the best matched endmembers to each of the materials for three of the five

datasets. Both Figures 2 and 4 indicate that the best matched endmembers are typically extracted for the material which dominates the satellite surface composition. The endmembers extracted from the dataset with all four satellites are all similar to the true materials. However, even in this case, CNMF and SKLD are unable to resolve aluminum and mylar.



(a) Satellite composed of 50% Aluminum, 17% Mylar, 17% Solar Cell, 16% White Paint.

(b) Satellite composed of 17% Aluminum, 16% Mylar, 50% Solar Cell, 17% White Paint.

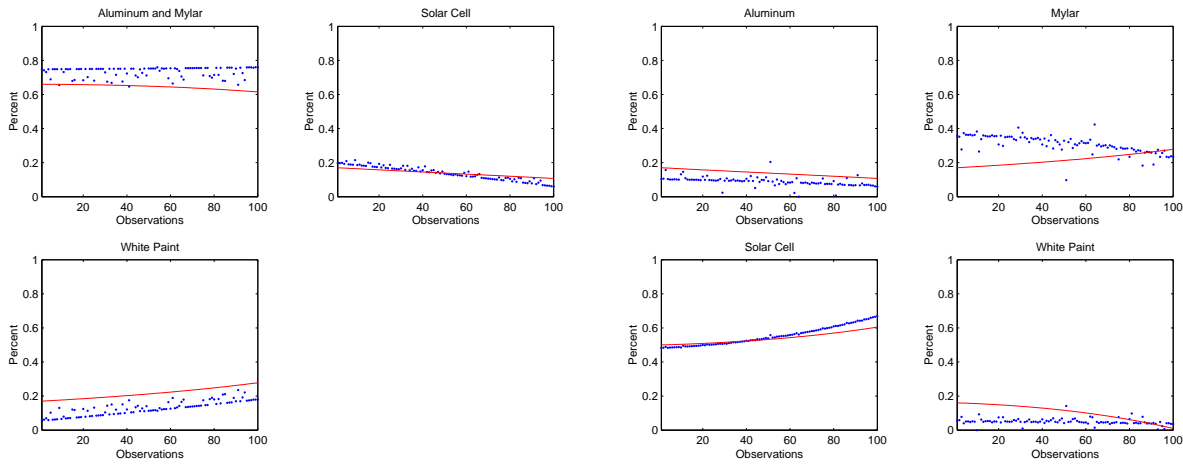


(c) All four simulated satellites.

Figure 4: Best endmembers extracted using CNMF with 1% noise and the smoothness penalty term, $\alpha = 1$ with 6 bases executed 20 times. Each dataset consisted of 100 observations for the simulated satellite. The three dimensional nature of each satellite was modeled by allowing each of the four components to vary as defined by a sine wave with random amplitude, frequency, and phase shift. 1% noise was added to the spectra.

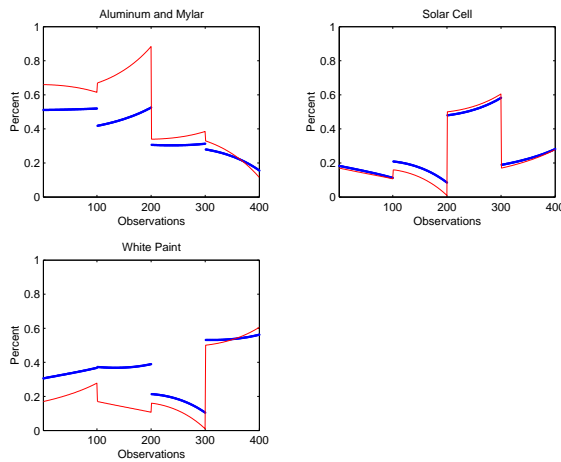
The fractional abundances of the endmembers were then calculated using iterative approximation as described in Subsection 3.3. The results are shown in Figure 5. In most cases, our method is effective at estimating both the fractional abundances as well as following the trend over the course of the 100 observations of each satellite as the abundances are allowed to vary. Figure 5(c) shows

again the difficulty of resolving aluminum, mylar, and white paint. The calculated fractional abundances for solar cell are quite good, while those for the other materials are less accurate, especially in the satellites dominated by aluminum and mylar.



(a) Simulated satellite composed of 50% Aluminum, 17% Mylar, 17% Solar Cell, 16% White Paint.

(b) Simulated satellite composed of 17% Aluminum, 16% Mylar, 50% Solar Cell, 17% White Paint.



(c) All four simulated satellites.

Figure 5: Percent compositions obtained using PMRNSD on the basis spectra in Figure 4. True composition is represented in red. The result of the approximation using PMRNSD is in blue.

5 Conclusions and Future Work

5.1 Effect of Dataset Size on Endmember Selection

More accurate results are achieved with the dataset of size $n = 400$ composed of the four simulated satellites, when compared to datasets containing only 100 traces of one satellite. This suggests that dataset diversity and size have an impact on the extraction of endmembers using CNMF.

Datasets with 10, 25, 100, and 1000 simulated spectra were constructed using random additive mixtures of the four laboratory spectra shown in Figure 1. CNMF was then executed ten times on each of these datasets to extract a set of six proposed endmember spectra. These proposed spectra were then compared with each of the four laboratory spectra used in the construction of the data by calculating the cosine of the angle between the normalized spectra. There is a marked improvement in the matching of endmembers with the true component spectra as the number of simulated observations used in the CNMF algorithm increases, see Figure 6.

CNMF was more successful at extracting endmembers when the data contained a larger number of spectra. CNMF, when executed on datasets with more distinct spectra, yielded visually smoother endmember spectra with higher matching indices with true endmember spectra. Datasets with fewer than 25 spectra resulted in noisier, more poorly resolved endmembers.

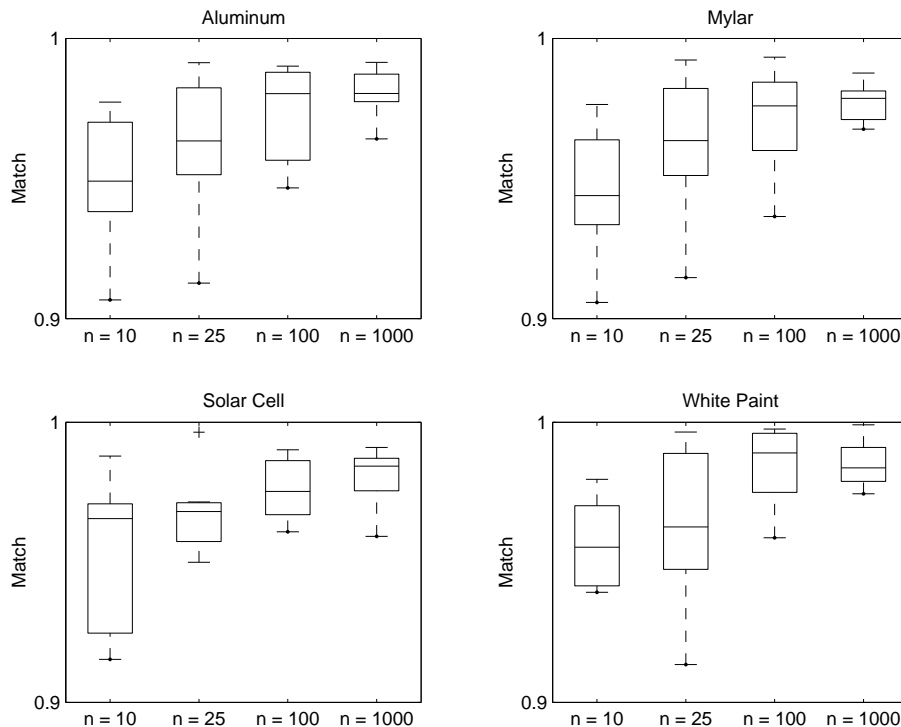


Figure 6: Box-and-whisker plots showing the average best matches between CNMF-extracted endmembers and the true laboratory-obtained component spectra for each of the four present materials. CNMF was executed ten times on each dataset. The size of the dataset is given by n . In each plot, the box represents the range from the lower quartile to the upper quartile, with the median line in between. The “whiskers” are 1.5 times the inter-quartile range.

5.2 Future Work

Future work on this ongoing project includes efforts to develop techniques to more strongly differentiate between certain spectral signatures, especially between aluminum and mylar. These additional methods include spectral feature encoding using wavelets, an approach that has been successful in other spectral unmixing applications [7].

References

- [1] A. Berman and R. Plemmons. *Non-Negative Matrices in the Mathematical Sciences*, SIAM Press Classics Series, Philadelphia, 1994.
- [2] M. Catral, L. Han, M. Neumann and R. Plemmons. “Reduced Rank Non-Negative Factorization for Symmetric Non-Negative Matrices”, preprint, 2003, to appear in *Linear Algebra and Applications*. See <http://www.wfu.edu/~plemmons>.
- [3] M.-A. Cauquy, M. Roggemann and T. Schultz. “Approaches for Processing Spectral Measurements of Reflected Sunlight for Space Situational Awareness”, *Proc. SPIE Conf. on Defense and Security*, Orlando, FL, 2004.
- [4] C.-I Chang. “An Information Theoretic-based Approach to Spectral Variability, Similarity, and Discriminability for Hyperspectral Image Analysis”, *IEEE Trans. Information Theory*, Vol. 46, pp. 1927-1932, 2000.
- [5] D. Donoho and V. Stodden. “When does Non-Negative Matrix Factorization Give a Correct Decomposition into Parts?”, preprint, Department of Statistics, Stanford University, 2003.
- [6] P. Hoyer. “Non-Negative Sparse Coding”, *Neural Networks for Signal Processing XII (Proc. IEEE Workshop on Neural Networks for Signal Processing)*, Martigny, Switzerland, 2002.
- [7] N. Keshava and J. Mustard. “Spectral Unmixing”, *IEEE Signal Processing Magazine*, pp. 44-57, January 2002.
- [8] K. Jorgensen et al. “Squigley Lines and Why They are Important to You”, *NASA Lincoln Space Control Conference*, Lexington, MA, March 2002.
- [9] D. Lee and H. Seung. “Learning the Parts of Objects by Non-Negative Matrix Factorization”, *Nature*, Vol. 401, pp. 788-791, 1999.
- [10] K. Luu, C. Matson, J. Snodgrass, M. Giffin, K. Hamada and J. Lambert. “Object Characterization from Spectral Data”, *Proc. AMOS Technical Conference*, Maui, HI, 2003.
- [11] J. G. Nagy, K. Palmer, and L. Perrone. “Iterative Methods for Image Deblurring: A Matlab Object Oriented Approach”, *Numerical Algorithms*, Vol. 36, No. 1, pp. 73-93, 2004.
- [12] V. P. Pauca, R. J. Plemmons, M. Giffin, and K. Hamada. “Mining Scientific Data for Non-Imaging Identification and Classification of Space Objects”, *Proc. AMOS Tech Conf.*, 2004.
- [13] V. P. Pauca, F. Shahnaz, M. Berry and R. Plemmons. “Text Mining using non-negative Matrix Factorizations”, *Proc. SIAM Inter. Conf. on Data Mining*, Orlando, April, 2004. See <http://www.wfu.edu/~plemmons>.
- [14] A. Plaza, P. Martinez, R. Perez and J. Plaza. “A Quantitative and Comparative Analysis of Endmember Extraction Algorithms from Hyperspectral Data”, *IEEE Trans. on Geoscience and Remote Sensing*, Vol. 42, No. 3, pp. 650-663, 2004.